Shallow Acceptor of Phosphorous Doped in $MoSe_2$ Monolayer

*Yipu Xia, Junqiu Zhang, Zhoubin Yu, Yuanjun Jin, Hao Tian, Yue Feng, Bin Li, Wingkin Ho, Chang Liu, Hu Xu, Chuanhong Jin, and Maohai Xie**

Y. Xia, J. Zhang, Y. Jin, H. Tian, W. Ho, Prof. M. Xie

Physics Department, The University of Hong Kong, Pokfulam Road, Hong Kong, 999077, China

E-mail: mhxie@hku.hk

Z. Yu and Prof. C. Jin

State Key Laboratory of Silicon Materials, School of Materials and Engineering, Zhejiang University, Hangzhou, Zhejiang, 310027, China

Y. Jin, H. Tian, Y. Feng, Dr. B. Li, Prof. C. Liu and Prof. H. Xu,

Department of Physics, Southern University of Science and Technology, Shenzhen, Guangdong 518055, China

KEYWORDS: Doping, TMD monolayer, MBE, STEM, STM

ABSTRACT

Tuning the conductivity and other electronic properties by doping in ultrathin layers of transition-metal dichalcogenides is of great scientific and practical interests. As of traditional semiconductors, controllable doping is essential for device applications of the materials. Here hole doping in epitaxial $MoSe_2$ by phosphorus (P) are reported, where substitutional P at the Se sites act as shallow acceptors. P substituting Se in $MoSe_2$ is identified by annular dark field scanning transmission electron microscopy, Auger electron spectroscopy, and X-ray photoelectron spectroscopy. Scanning tunneling spectroscopy and ultraviolet photoemission spectroscopy reveal in-gap defect states and Fermi-level shifts, suggesting the hole doping effect of substitutional P. Combining with density functional theory calculation and partial charge analysis, the binding energies of impurity levels of group V elements in $MoSe_2$ monolayer are elucidated, where the dopant energy level becomes shallower with increasing atomic mass.

1. Introduction

Two-dimensional (2D) transition metal dichalcogenides (TMDs), such as $MoSe_2$ monolayer (ML), are direct-gap semiconductors that have attracted great research interests in recent years. They exhibit many interesting electronic, optoelectronic, spin- and valley-electronic properties and hold great device promises.[1-7] Similar to traditional semiconductors, doping of TMDs can be critical in order to tune their p- and n-type conductivities, necessary for device applications.[8-10] Three primary doping strategies have been applied to TMDs: charge transfer by gating, surface modification and substitutional doping.[11-16] Charge transfer via nitrogen dioxide and ion gel gate dielectrics have been experimented to achieve both p- and n-type doping.[3, 17] Surface modifications such as by potassium adsorption have led to electron doping and induced the phase transition from semiconductor to metal,[18-20] while adsorption of some other metal nanoparticles such as Au, Ag, Pd and Pt have been shown to give rise to p-type doping effect.[21] Substitutional doping is intrinsically more stable and reliable than surface adsorption.[22] P-type MoS_2 and WS_2 by substituting Mo with Nb or Ta have been reported.[23-28] Electron doping by substituting Mo by Re has been demonstrated as well, and a phase transition from 2H to 1T' was noted when the doping level is high.[11, 29-32] Besides substituting the metal atoms, dopants replacing the chalcogen atoms in TMDs may also be introduced, such as the p-type dopant of nitrogen in $MoSe_2$ and the n-type dopant of Cl in MoS_2 and WS_2, etc. [6], [33] Isoelectronic doping, e.g., Se in MoS_2, has also been demonstrated, where the energy bandgap is tuned by changing Se concentrations.[34]

In this work, phosphorus (P) doping in $MoSe_2$ monolayer during growth by molecular beam epitaxy (MBE) is investigated, revealing an effective hole doping effect. Combining annual dark field scanning transmission electron microscopy (ADF-STEM), energy dispersive X-ray

spectroscopy (EDS), Auger electron spectroscopy (AES), X-ray/ultraviolet photoelectron spectroscopy (XPS/UPS), angle resolved photoemission spectroscopy (ARPES), scanning tunneling microscopy and spectroscopy (STM/S), we establish that P substitutes Se in epitaxial $MoSe_2$ and causes downshifts of the Fermi level. An in-gap acceptor state close to the valence band maximum (VBM) is observed, consistent with our density functional theory (DFT) calculations.

2. Results and Discussion

2.1. Substitutional P at Se sites in $MoSe_2$

P doping in $MoSe_2$ monolayer is achieved during MBE, where P is co-deposited with Mo and Se on highly oriented pyrolytic graphite (HOPG) or graphene-on-SiC substrate. By changing the flux of P relative to that of Mo and Se during deposition, the doping level can be tuned (refer to Supporting Information 1). **Figure 1(a)** presents an ADF-STEM image of a P-doped sample, in which inversion domain boundary (IDB) defects are highlighted by semi-transparent blue lines. Dense network of IDBs in epitaxial $MoSe_2$ grown by MBE has been consistently shown.[2, 35-39] Co-deposition of Se and P apparently does not change the situation. Figure 1(b) shows a STM image of the P-doped $MoSe_2$ sample. Besides retaining the dense IDBs, P doping does not affect the hexagonal structure of pristine $MoSe_2$, nor generates any apparent phosphorus-related structures within or on the surface of $MoSe_2$ as far as we observe. The hexagonal domains are not degraded by P co-deposition and the IDBs are not disrupted either.

Figure 2(a) shows a high-resolution ADF-STEM image of another P-doped $MoSe_2$ sample prepared at a slightly higher P/Se flux ratio of ~4.5, in which Se and P atoms are marked by

green and yellow circles based on the contrast analysis as exemplified in Figure 2(b). As seen, except for an intensity peak pointed by the red arrow in Figure 2(b), peaks of high and low intensities alternate along the line A-B drawn in Fig, 2(a), which reflect Se and Mo sites respectively in 2*H*-$MoSe_2$ (note that the ADF-STEM contrast is proportional to $Z^{1.6\text{-}2.0}$, where Z is the atomic number, and at Se site there are two Se atoms). The red-arrow-pointed peak corresponds to one of the Se sites, and its lower intensity than the other Se sites may then be attributed to a Se vacancy (V_{Se}) or a P atom substituting a Se (P_{Se}) at this very site (see Figure 2(c) of schematic illustration).[40] To further distinguish between P_{Se} and V_{Se}, we performed simulations using the QSTEM® software of $MoSe_2$ monolayers containing the above two defects.[41] The simulated results are shown in Figures 2(d) and 2(e), respectively. One notes that for the P_{Se} defect, the intensity is about 86% of that of Mo, whereas for the vacancy defect V_{Se}, it is ~66%. Experimentally, the measured intensity ratio between the defect site and Mo is 87%, which is consistent with the simulated result of the substitutional P_{Se} defect.

We however stress that the discrimination of Se-vacancy defects in sample by the intensity analysis based on the above simulation cannot be unambiguous or conclusive. In particular, it was reported that high-energy electron irradiation of the sample during STEM experiments would generate vacancy defects in $MoSe_2$.[42] To check this and to distinguish the two defects more unambiguously, we have compared samples with and without P-doping but otherwise grown under the same conditions and measured using the same STEM setting. The results are presented in Supporting Information 2, revealing firstly higher defect densities in P-doped samples. Second, we have continuously recorded STEM images over one and the same area of size 8×8 nm^2 of a sample and found two vacancies being generated during measurement of ~53 seconds. The preexisting defects were dominant, which were thus unlikely vacancies created

during the STEM experiments. Moreover, Se vacancies would behave as electron donors according to the DFT calculations (see Supporting Information 3), contradicting to our experimental observation that P-doped samples are p-type as presented later. In fact, in the image of Figure 2(a), we do observe some Se sites to exhibit even lower contrasts (e.g., marked by blue circles), which may well be ascribed to Se vacancies. Besides, our EDS measurements (see Figure 2(f)) did reveal P-Kα peaks and the peak intensity varied with changing P/Se flux ratio (see Supporting Information 1). Based on the intensity ratio between the P-Kα and Mo-Lα peaks, we may roughly estimate the atomic concentration of P in sample. For instance, it is about 2% for the one grown at P/Se ~ 4.5. AES and XPS measurements of P-doped samples also show characteristic peaks associated with P (Figures 2g and 2h).[43, 44] Analysis of the Mo $3d_{5/2}$ peak in the XPS spectrum also shows an apparent shoulder at ~0.6 eV above the main peak at ~228.6 eV (Figure 2i), signifying Mo-P bonding. Our density functional theory (DFT) calculations of the projected density of state (PDOS) confirms the involvement of Mo_{3d} orbital when bonded with P atoms in $MoSe_2$ (Supporting Information 4). So, all of these point to the successful doping of P in $MoSe_2$ by substituting Se atoms during MBE.

In passing, it will be an interesting question whether the same substitutional doping can be achieved during chemical vapor deposition (CVD) of the TMDs. Firstly, the propensity of P incorporation in $MoSe_2$ during co-deposition of P, Se and Mo, as revealed in the above experiments, remains favoring P doping in $MoSe_2$ even for CVD. On the other hand, we wish to comment that the adsorption rate of P decreases rapidly with increasing temperature, so it is necessary to maintain a relatively low temperature during growth. This may contradict to the temperature requirement for effective cracking the precursor molecules used in CVD, so a balance and/or choice of adequate precursors will be needed. Another complication arises from

the effect of the radical by-products in the CVD chamber, if reacted strongly with P, effective P doping may also be hindered. So transferability of the above experimental findings in the MBE to CVD is not apparent, and more systematic studies of doping in TMD during CVD will be required and called upon. In the following, we shall continue our discussion on the electronic properties the substitutional P dopants bring to the $MoSe_2$ ML grown by MBE.

2.2. Acceptor states and Fermi-level tuning by P-doping

To examine the electronic properties and effects of P doping in $MoSe_2$, we carried out spectroscopic measurements using (AR)PES and STS, and **Figure 3** presents some of the results evidencing a hole-doping effect, e.g., the Fermi level shift and the appearance of defect states close to the VBM. In other words, substitutional phosphorous acts as acceptors in $MoSe_2$. Specifically, Figures 3(a) and 3(b) show two ARPES from an undoped and P-doped $MoSe_2$ monolayer, respectively. With the P/Se flux ratio of ~4.5 and the estimated atomic concentration of P being ~2%, the valence band edge of the P-doped $MoSe_2$ is seen to be upshifted by about 0.3 eV relative to the Fermi level, $E_F = 0$ eV, or equivalently the E_F downshifted by the same amount. UPS measurements confirm the same (refer to Figure 3c). In addition, it is shown that changing the flux ratio from 4.5 to 3.2 has led to a reduced E_F shift of ~0.1 eV relative to that of the undoped sample.

Figures 3(d) and 3(e) present two topographic STM images of the P-doped $MoSe_2$ sample grown at P/Se~4.5, measured at 77K over one and the same area but under different bias conditions. As seen, at the sample bias of -1.0 V (Figure 3e), a defect is clearly seen and manifests by a bright feature of 3-fold symmetry. At -0.5 eV, the defect shows no structural feature (Figure 3d). The apparent contrast enhancement in the upper-left region in Figure 3(d)

may not be associated with the defect seen in Figure 3(e) but a cluster close-by (out of the view but can be seen from a large-area image presented in Supporting Information 5). By making reference to the ADF-STEM result presented earlier, one notes that P substitutional doping would not break the original lattice structure. On the other hand, it introduces new electronic states (see below) with spatial distribution depicted in Figure 3(g), a simulated STM image of the P_{Se} defect. Figure 3(f) presents a set of STS spectra taken from a P-doped $MoSe_2$ monolayer close to (red) and away from (black) the defect. For comparison, a spectrum taken from a pristine $MoSe_2$ ML grown on the same HOPG substrate is also given (blue line). As the two samples should have the same Fermi energy as pinned by the substrate, comparing the spectra of the pristine and P-doped $MoSe_2$ (i.e., blue vs. black curves in Figure 3f) reveals an apparent upward shift of the band edges relative to the Fermi level in the P-doped sample, indicating a hole doping effect. The spectrum taken at the defect (red curve) shows a narrower gap as well as a DOS peak at about -1 V, very close to the valance band edge. We believe the latter represents the acceptor state of P, which is not present in undoped $MoSe_2$ according to both experimental and theoretical studies.[19, 45] This DOS peak is seen to almost overlap with the valance band edge, but if measured relative to the VBM of intrinsic $MoSe_2$, i.e., the black curve in Figure 3(f) obtained at a defect-free region of the same sample, it is about 0.3 eV above the VBM. This is a much shallower acceptor than that of nitrogen (N) in $MoSe_2$ as reported before (~0.6 eV).[6] The likelihood of some other possible candidates of the defects, such as Se vacancy or P-adatom, may be excluded as according to our DFT calculations, these defects do not give rise to hole doping, nor the DOS that matches the experiment (see Supporting Information 3).

By Boltzmann statistics, one estimates that a Fermi level shift of 0.3 eV as shown in Figure 1(b) would correspond to a hole doping of only $\sim 2.3 \times 10^9$ atoms/cm^3, far less than the estimated

atomic concentration of 2% from the EDS result (see Supporting Information 6). There can be many reasons for this discrepancy. Firstly, despite shallower than N dopant, the activation energy of ~0.3 eV as revealed by the above STS measurement remains appreciable, so at room-temperature of the ARPES measurements, only a minute proportion of $\sim 1 \times 10^{-5}$ of the substitutional P atoms would be thermally ionized and contribute to holes. Secondly, among the ~2% P atoms estimated by EDS measurement, being highly inaccurate itself, not all are affirmed substitutional and if some are at, e.g., interstitial or adsorption sites, they would not contribute to holes but compensating electrons instead. Although no experimental evidence exists suggesting the presence of interstitial or adsorbed P, a high density of IDBs would have also affected the carrier density in film. Indeed, our undoped samples all show background electron doping and manifest by the above mid-gap Fermi levels. These background electrons will inevitably compensate the holes introduced by P-doping. Finally, there exists an apparent gap narrowing at the defect as seen in Figure 3(f). It can be caused either by a resonance of the defect states with the valance band, or by a strain introduced by doping. A non-uniform strain distribution across the film can result in a bandgap variation (see Supporting Information 8).

2.3 DFT of doping by group V elements in $MoSe_2$

We now discuss the ionization energies of group-V dopants in $MoSe_2$ monolayer. It is known that in 2D systems, dielectric screening is much reduced, which accounts for the giant exciton binding energy in TMD monolayers.[46] The same applies to shallow dopants where the ionization energy can be enhanced by the reduced effective dielectric constant ϵ^{2D} in 2D systems.[47] Therefore, doping by impurity in 2D films is generally not very effective. On the other hand, owing to the good structural stability, doping by impurity remains attractive and

identifying the most suitable dopants with low ionization energies is critical. To this end, one may follow a guideline that impurity atoms having the same core levels as that of the substituted host atoms, and if the impurity band originates from one having the p-symmetry envelope rather than s-symmetry, tend to have shallow defect energy levels.[48] In the case of group-V dopants in monolayer $MoSe_2$, such as P, our DFT calculations (**Figure 4a** and 4b for a pristine and P-doped $MoSe_2$) show that the dopant introduces an impurity band near the top of the valence band, and at a concentration of ~2% (i.e., one dopant atom over the supercell size of 4×4), the Fermi level becomes pinned at the defect band. Apart from this, no significant change is brought about within but close to the VBM (and CBM). Lowering the concentration to ~1% P in our calculation (through enlarging the supercell size) does not lead to much change of the defect state energy (see Supporting Information 7). In our ARPES experiments of P-doped samples, no impurity band can be explicitly observed, possibly due to the relatively low impurity concentrations in samples. It is perhaps due to the same reason that the Fermi energy in real sample is far from the VBM. One comment is in place though that one needs to be careful when comparing the theory with experiments in absolute terms, such as the energy positions, as it is well known that the DFT using Perdew-Burke-Ernzerbof (PBE) pseudopotentials significantly underestimate the energy gaps.[49, 50] In addition, our DFT calculations have not included the HOPG (or graphene) substrate, which is obviously present in experiment, and the latter may have caused Fermi level change due to charge transfer.[51] Despite the above, qualitative features such as the valence band structures are found to agree well between the experiment and calculations.

We further compare three group-V dopants: N, P and As, by DFT calculations and find indeed that the impurity bands become shallower with increasing atomic number where their core levels increasingly resemble that of Se in the $MoSe_2$ host (see Supporting Information 4). This trend is

consistent with our experiments of N and P doping, where the former has been previously reported to have an ionization energy of ~0.66 eV above the VBM,[6] much deeper than the ~0.3 eV observed here for P dopant. PDOS analyses show that the impurity bands originate mainly from the hybridization of the p_z orbital of the dopant atom and the d_{z^2} orbitals of Mo. The s-orbital of the dopant plays little part in defect state formation (refer to the Supporting Information 4). Figure 4(c) compares the energy levels of bonding and antibonding states between Mo d_{z^2} and X p_z (X refers to N, P or As). As the atomic number of X increases, the bond length of Mo-X becomes larger, which results in a decrease in the overlap integral between Mo d_{z^2} and X p_z orbitals, thus their bonding becomes weaker. According to a recent first-principle study on doping in 2D semiconductors, the out-of-plane partial charge has a significant influence on doping characteristics.[52] In Figures 4(d) and 4(e), we compare the partial charge densities of N and P dopants in $MoSe_2$. It is seen that while the defect states in N-doped $MoSe_2$ distribute mainly within the 2D layer, significant out-of-plane components can be discerned in P-doped $MoSe_2$. Such a difference might be partly responsible for the different ionization energies between N and P doped in $MoSe_2$.

3. Conclusions

To conclude, we have demonstrated P doping in epitaxial $MoSe_2$ monolayer by co-deposition of P, Se and Mo during MBE. Combining ADF-STEM, EDS, XPS, AES and STM/S, we establish that P atoms substitute Se in $MoSe_2$ and act as acceptors as evident from the Fermi level shift as well as the appearance of impurity states in the gap but close to VBM. The doping level can be tuned by changing the P/Se flux ratio. Both experiments and DFT calculations show that P dopant has a relatively shallow energy level and is thus an effective hole dopant in $MoSe_2$.

4. Experimental Section

Molecular beam epitaxy of $MoSe_2$ and P-doping

Growths of P-doped $MoSe_2$ monolayer on graphene or HOPG were carried out in an Omicron UHV system having the background pressure of low 10^{-10} torr. The flux of Mo was generated from e-beam evaporator and that of Se was provided from a conventional Knudsen cell. P flux was generated by the decomposition of high purity InP by an e-beam too. Before $MoSe_2$ deposition and P doping, freshly cleaved HOPG or epitaxial graphene substrate was prepared. For the latter, it was achieved by heating a SiC wafer at ~1100℃ in a Si flux. The substrate temperature used for P-doped $MoSe_2$ deposition was 400 ℃ and the deposition rate was 0.5 MLs/hr. Fluxes of Se, Mo and P were controlled by the Knudsen cell temperature or power supplied to the e-beam cells and measured by beam-equivalent pressures and/or the ion current readout from the e-cells. In situ RHEED was operated at 10 keV.

Scanning transmission electron microscopy and electron energy loss spectroscopy

Specimens of P-doped $MoSe_2$ on HOPG were prepared by micromechanical exfoliation processes, and transferred onto a tungsten TEM grid with lacey carbon film for the ADF-STEM and EDS measurements ex situ. The paraffin wax used in the micromechanical exfoliation process were repeatedly washed by acetone. ADF-STEM was performed in a probe-corrected STEM (FEI Titan Chemi STEM) operated at 200 kV. The convergence angles for ADF-STEM and EDS were 30 mrad and 21.4 mrad, respectively. The minimal acceptance angle of the ADF detector was set at ~53 mrad.

Ultraviolet and X-ray photoelectron spectroscopy, angle resolved photoemission spectroscopy

Both UPS and XPS measurements were carried out in a separate chamber vacuum connected to MBE rightly after the growth. A high intensity helium discharge source (He-I = 21.2eV) was used for the UPS measurements, while for XPS, the X-ray source was a twin-anode (Mg/Al) source from VG (Model XR3E2). Photoelectrons were analyzed by SPECS PHOIBOS 100 MCD-5 electron analyzer. The ARPES experiments at room temperature were conducted using a laboratory-based ARPES system consisted of a SPECS PHOIBOS 150 electron analyzer and a UVLS-600 UV lamp. The base pressures in all were in the low $10^{-9} \sim 10^{-10}$ mbar range.

Scanning tunneling microscopy/spectroscopy

STM/STS measurements were carried out at 77K in a Unisoku scanning tunneling microscope (USM1500). It operated at the constant current mode with the tunneling current of 100pA.

Supporting Information

Supporting Information is available from the Wiley Online Library or from the author.

Acknowledgments

Y.X. and J.Z. contribute equally to this work. We thank Bo Wang for fruitful discussions. The work is financially supported by a General Research Fund (No. 17327316) and a Collaborative Research Fund (C7036-17W) from the Research Grant Council, Hong Kong Special Administrative Region, and a NSFC/RGC joint research grant (No. N_HKU732/17; 51761165024).

Reference

References

[1] K. F. Mak, C. Lee, J. Hone, J. Shan, T. F. Heinz, Phys Rev Lett 2010, 105, 136805.
[2] H. Liu, L. Jiao, F. Yang, Y. Cai, X. Wu, W. Ho, C. Gao, J. Jia, N. Wang, H. Fan, W. Yao, M. Xie, Physical Review Letters 2014, 113, 066105.
[3] Q. H. Wang, K. Kalantar-Zadeh, A. Kis, J. N. Coleman, M. S. Strano, Nat Nanotechnol 2012, 7, 699.
[4] X. Xu, W. Yao, D. Xiao, T. F. Heinz, Nature Physics 2014, 10, 343.
[5] L. Jiao, H. J. Liu, J. L. Chen, Y. Yi, W. G. Chen, Y. Cai, J. N. Wang, X. Q. Dai, N. Wang, W. K. Ho, M. H. Xie, New Journal of Physics 2015, 17, 053023.
[6] Y. P. Xia, B. Wang, J. Q. Zhang, Y. Feng, B. Li, X. B. Ren, H. Tian, J. P. Xu, W. K. Ho, H. Xu, C. Liu, C. H. Jin, M. H. Xie, 2d Materials 2018, 5, 041005.
[7] W. Jolie, C. Murray, P. S. Weiß, J. Hall, F. Portner, N. Atodiresei, A. V. Krasheninnikov, C. Busse, H.-P. Komsa, A. Rosch, T. Michely, Physical Review X 2019, 9, 011055.
[8] Y. Gong, J. J. N. M. Lin, 2014, 13, 1135.
[9] H. P. Komsa, J. Kotakoski, S. Kurasch, O. Lehtinen, U. Kaiser, A. V. Krasheninnikov, Phys Rev Lett 2012, 109, 035503.
[10] D. Jariwala, V. K. Sangwan, L. J. Lauhon, T. J. Marks, M. C. Hersam, ACS Nano 2014, 8, 1102.
[11] K. Dolui, I. Rungger, C. D. Pemmaraju, S. Sanvito, Physical Review B 2013, 88, 075420.
[12] D. Kiriya, M. Tosun, P. D. Zhao, J. S. Kang, A. Javey, Journal of the American Chemical Society 2014, 136, 7853.
[13] S. Mouri, Y. Miyauchi, K. Matsuda, Nano Letters 2013, 13, 5944.
[14] P. Rastogi, S. Kumar, S. Bhowmick, A. Agarwal, Y. S. Chauhant, Journal of Physical Chemistry C 2014, 118, 30309.
[15] M. Amani, D. H. Lien, D. Kiriya, J. Xiao, A. Azcatl, J. Noh, S. R. Madhvapathy, R. Addou, S. Kc, M. Dubey, K. Cho, R. M. Wallace, S. C. Lee, J. H. He, J. W. Ager, 3rd, X. Zhang, E. Yablonovitch, A. Javey, Science 2015, 350, 1065.
[16] M. Amani, P. Taheri, R. Addou, G. H. Ahn, D. Kiriya, D. H. Lien, J. W. Ager, 3rd, R. M. Wallace, A. Javey, Nano Lett 2016, 16, 2786.
[17] S. Das, H. Y. Chen, A. V. Penumatcha, J. Appenzeller, Nano Lett 2013, 13, 100.
[18] H. Fang, M. Tosun, G. Seol, T. C. Chang, K. Takei, J. Guo, A. Javey, Nano Lett 2013, 13, 1991.
[19] Y. Zhang, T. R. Chang, B. Zhou, Y. T. Cui, H. Yan, Z. Liu, F. Schmitt, J. Lee, R. Moore, Y. Chen, H. Lin, H. T. Jeng, S. K. Mo, Z. Hussain, A. Bansil, Z. X. Shen, Nat Nanotechnol 2014, 9, 111.
[20] B. Lei, Y. Pan, Z. Hu, J. Zhang, D. Xiang, Y. Zheng, R. Guo, C. Han, L. Wang, J. Lu, ACS nano 2018, 12, 2070.
[21] D. Sarkar, X. Xie, J. Kang, H. Zhang, W. Liu, J. Navarrete, M. Moskovits, K. Banerjee, Nano Lett 2015, 15, 2852.
[22] R. Mukherjee, H. Chuang, M. Koehler, N. Combs, A. Patchen, Z. Zhou, D. Mandrus, Physical Review Applied 2017, 7, 034011.
[23] J. Suh, T. E. Park, D. Y. Lin, D. Fu, J. Park, H. J. Jung, Y. Chen, C. Ko, C. Jang, Y. Sun, R. Sinclair, J. Chang, S. Tongay, J. Wu, Nano Lett 2014, 14, 6976.

[24] M. R. Laskar, D. N. Nath, L. Ma, E. W. Lee, C. H. Lee, T. Kent, Z. Yang, R. Mishra, M. A. Roldan, J.-C. Idrobo, Applied Physics Letters 2014, 104, 092104.
[25] X. J. Chua, J. Luxa, A. Y. S. Eng, S. M. Tan, Z. Sofer, M. Pumera, Acs Catalysis 2016, 6, 5724.
[26] S. Das, M. Demarteau, A. Roelofs, Applied Physics Letters 2015, 106, 173506.
[27] J. Gao, Y. D. Kim, L. Liang, J. C. Idrobo, P. Chow, J. Tan, B. Li, L. Li, B. G. Sumpter, T. M. Lu, Advanced Materials 2016, 28, 9735.
[28] Y. J. Fu, M. S. Long, A. Y. Gao, Y. Wang, C. Pan, X. W. Liu, J. W. Zeng, K. Xu, L. L. Zhang, E. F. Liu, W. D. Hu, X. M. Wang, F. Miao, Applied Physics Letters 2017, 111, 043502.
[29] K. H. Zhang, B. M. Bersch, J. Joshi, R. Addou, C. R. Cormier, C. X. Zhang, K. Xu, N. C. Briggs, K. Wang, S. Subramanian, K. Cho, S. Fullerton-Shirey, R. M. Wallace, P. M. Vora, J. A. Robinson, Advanced Functional Materials 2018, 28, 1706950.
[30] V. Kochat, A. Apte, J. A. Hachtel, H. Kumazoe, A. Krishnamoorthy, S. Susarla, J. C. Idrobo, F. Shimojo, P. Vashishta, R. Kalia, A. Nakano, C. S. Tiwary, P. M. Ajayan, Advanced Materials 2017, 29, 1703754.
[31] T. Hallam, S. Monaghan, F. Gity, L. Ansari, M. Schmidt, C. Downing, C. P. Cullen, V. Nicolosi, P. K. Hurley, G. S. Duesberg, Applied Physics Letters 2017, 111, 203101.
[32] S. Z. Yang, Y. Gong, P. Manchanda, Y. Y. Zhang, G. Ye, S. Chen, L. Song, S. T. Pantelides, P. M. Ajayan, M. F. Chisholm, Advanced Materials 2018, 30, 1803477.
[33] L. Yang, K. Majumdar, H. Liu, Y. Du, H. Wu, M. Hatzistergos, P. Y. Hung, R. Tieckelmann, W. Tsai, C. Hobbs, P. D. Ye, Nano Lett 2014, 14, 6275.
[34] Y. Gong, Z. Liu, A. R. Lupini, G. Shi, J. Lin, S. Najmaei, Z. Lin, A. L. Elias, A. Berkdemir, G. You, H. Terrones, M. Terrones, R. Vajtai, S. T. Pantelides, S. J. Pennycook, J. Lou, W. Zhou, P. M. Ajayan, Nano Lett 2014, 14, 442.
[35] S. Barja, S. Wickenburg, Z.-F. Liu, Y. Zhang, H. Ryu, M. M. Ugeda, Z. Hussain, Z.-X. Shen, S.-K. Mo, E. Wong, Nature Physics 2016, 12, 751.
[36] Y. Ma, H. C. Diaz, J. Avila, C. Chen, V. Kalappattil, R. Das, M.-H. Phan, T. Čadež, J. M. Carmelo, M. C. Asensio, Nature communications 2017, 8, 14231.
[37] O. Lehtinen, H. P. Komsa, A. Pulkin, M. B. Whitwick, M. W. Chen, T. Lehnert, M. J. Mohn, O. V. Yazyev, A. Kis, U. Kaiser, A. V. Krasheninnikov, ACS Nano 2015, 9, 3274.
[38] Z. Lin, B. R. Carvalho, E. Kahn, R. T. Lv, R. Rao, H. Terrones, M. A. Pimenta, M. Terrones, 2d Materials 2016, 3, 022002.
[39] J. Lin, S. T. Pantelides, W. Zhou, ACS Nano 2015, 9, 5189.
[40] J. Hong, C. Wang, H. Liu, X. Ren, J. Chen, G. Wang, J. Jia, M. Xie, C. Jin, W. Ji, J. Yuan, Z. Zhang, Nano Lett 2017, 17, 6653.
[41] C. T. Koch, *Determination of core structure periodicity and point defect density along dislocations*, 2002.
[42] T. Lehnert, O. Lehtinen, G. Algara–Siller, U. Kaiser, Applied Physics Letters 2017, 110, 033106.
[43] P. Xiao, M. A. Sk, L. Thia, X. M. Ge, R. J. Lim, J. Y. Wang, K. H. Lim, X. Wang, Energy & Environmental Science 2014, 7, 2624.
[44] Y. Huang, J. Ge, J. Hu, J. Zhang, J. Hao, Y. Wei, Advanced Energy Materials 2018, 8, 1701601.
[45] H. Liu, L. Jiao, F. Yang, Y. Cai, X. Wu, W. Ho, C. Gao, J. Jia, N. Wang, H. Fan, Physical review letters 2014, 113, 066105.
[46] D. Y. Qiu, H. Felipe, S. G. Louie, Physical review letters 2013, 111, 216805.

[47] A. Kumar, P. Ahluwalia, Physica B: Condensed Matter 2012, 407, 4627.
[48] P. Y. Yu, M. Cardona, *Fundamentals of semiconductors: physics and materials properties*, Springer, 2010.
[49] J. P. Perdew, International Journal of Quantum Chemistry 1985, 28, 497.
[50] M. Chan, G. Ceder, Physical review letters 2010, 105, 196403.
[51] S. Singh, C. Espejo, A. H. Romero, Physical Review B 2018, 98, 155309.
[52] C. Zhang, C.-P. Chuu, X. Ren, M.-Y. Li, L.-J. Li, C. Jin, M.-Y. Chou, C.-K. Shih, Science advances 2017, 3, e1601459.
[53] W. Ku, T. Berlijn, C.-C. Lee, Physical review letters 2010, 104, 216401.

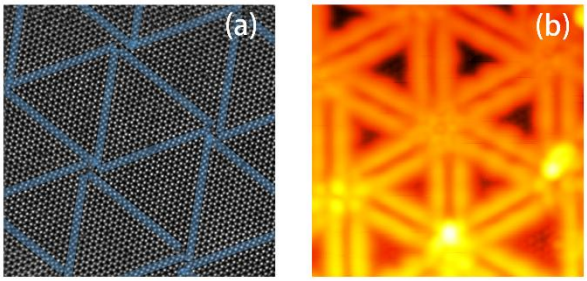

Figure 1. Structure of P-doped $MoSe_2$ monolayer. (a) ADF-STEM image (size: 12×12 nm^2) and (b) STM image (size: 10×10 nm^2, sample bias: -1.0 V) of P-doped $MoSe_2$ with a P/Se flux ratio of ~3.2.

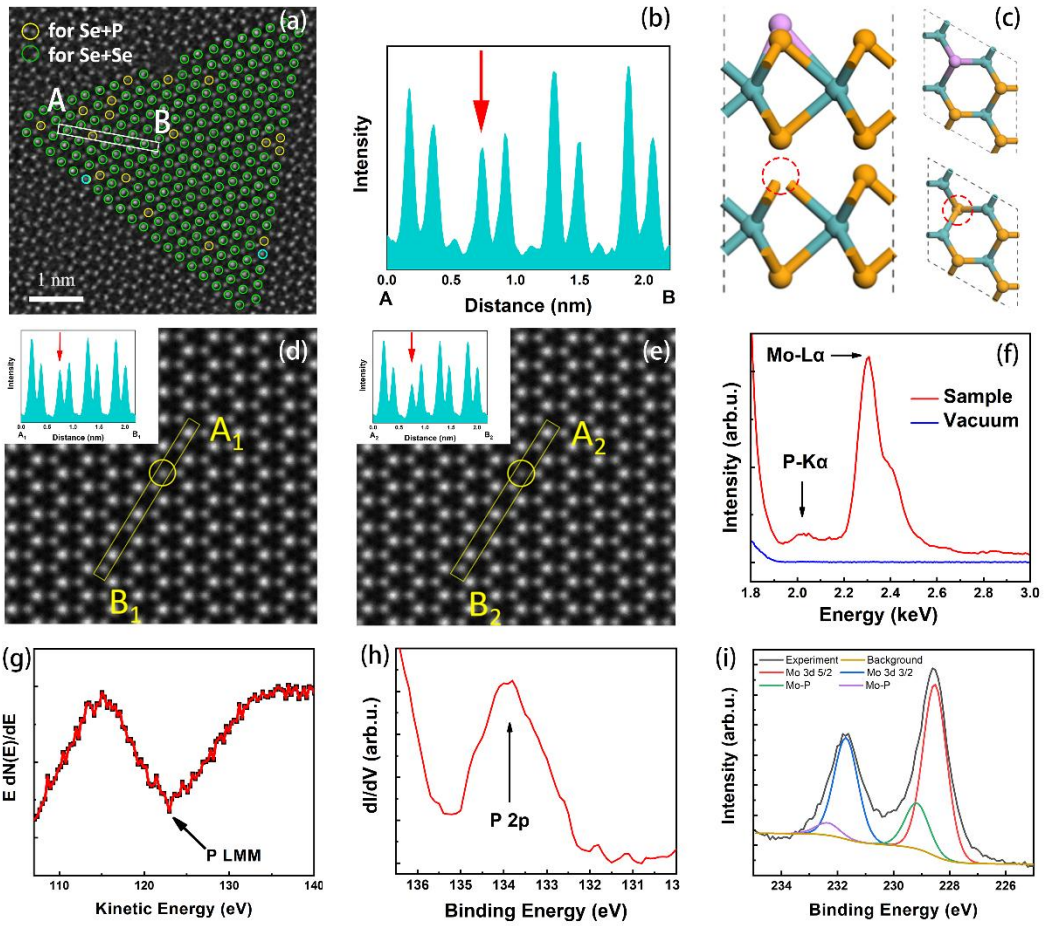

Figure 2. STEM/EDS/AES/XPS results showing P substitutional doping in $MoSe_2$. (a) High-resolution ADF-STEM image of a P-doped $MoSe_2$ grown using a P/Se flux ratio of ~4.5, where green and yellow circles label Se and P_{Se} sites, respectively, and blue circles label the V_{Se} sites. (b) Intensity profile along the boxed region A-B in (a). Note a reduced intensity peak at one of Se sites pointed by a red arrow, which corresponds to a P_{Se} defect. (c) Schematic drawings in side-view (left) and top-view (right) of the two defects at Se site in $MoSe_2$: P_{Se} (top) and V_{Se} (bottom). (d-e) QSTEM simulated ADF-STEM images and corresponding intensity profiles along boxed regions containing a P_{Se} (d) or a V_{Se} (e) at the circled site, respectively. (f) EDS revealing the P-$K\alpha$ and Mo-$L\alpha$ peaks. (g) AES and (h) XPS spectra taken from a P-doped

sample, and the arrows point to P-related peaks. (i) XPS showing Mo_{3d} core level peaks, revealing Mo-P and Mo-Se bonding.

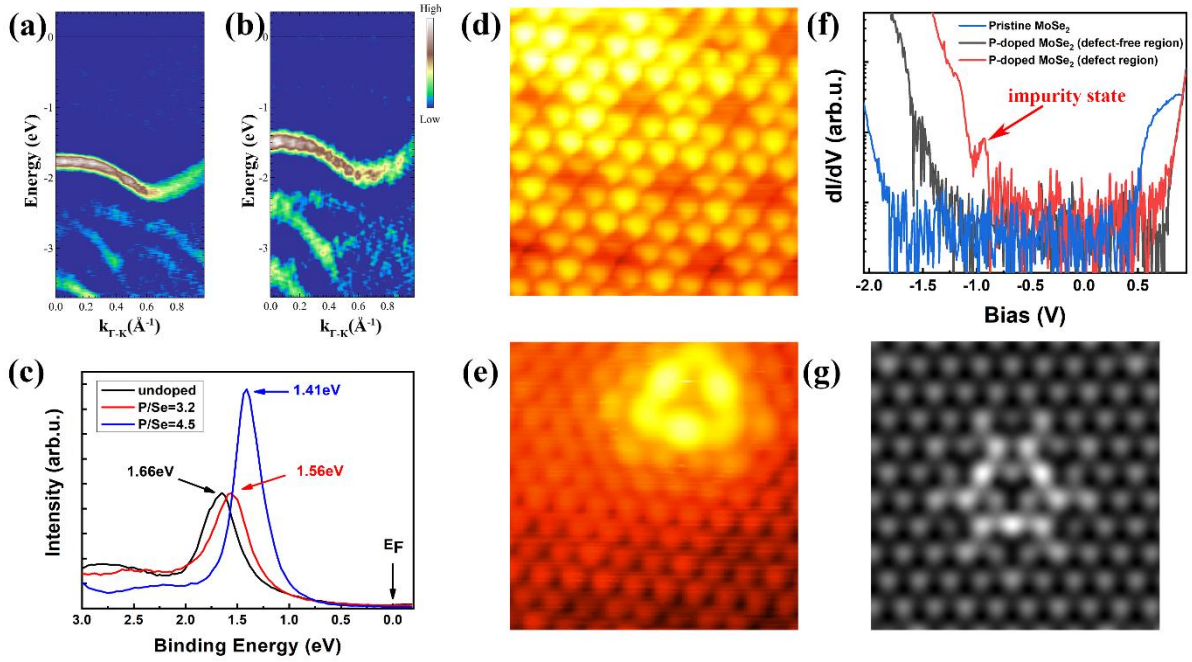

Figure 3. Hole doping effect of P in $MoSe_2$. (a,b) Second-derivate ARPES spectra of (a) undoped and (b) P-doped (P/Se Flux ratio: ~4.5) $MoSe_2$ monolayer, showing an upper shift of the VBM relative to E_F (0 eV) in the P-doped sample. Equivalently, it represents a downshift of E_F relative to VBM. (c) UPS of the undoped, light (P/Se flux ratio ~3.2) and heavy (P/Se ~ 4.5) P-doped $MoSe_2$, showing the different magnitudes of the E_F shifts. The peaks mark states close to the VBM of $MoSe_2$. (d,e) STM images (3×3 nm^2) of the same area of a P-doped sample taken at different sample bias of -0.5 V (d) and -1.0 V (e). (f) STS spectra taken on pristine, and P-doped $MoSe_2$ but at defect-free and the defect sites, respectively. The tunneling current was 100 pA. (g) Simulated STM image of a P_{Se} defect in $MoSe_2$ (size: 3.2×3.2 nm^2, energy: -0.2eV).

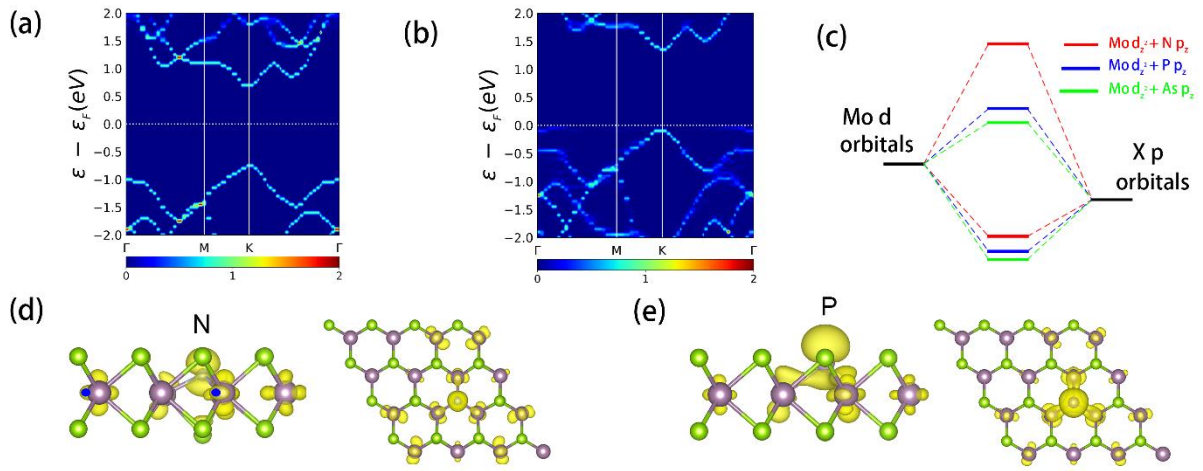

Figure 4. DFT calculations of doped $MoSe_2$ monolayer by group-V elements. (a-b) Energy bands of undoped and P-doped $MoSe_2$ monolayer. An impurity band appears close to valence band edge upon doping. Note that for the latter, one P in a 4×4 supercell is assumed, corresponding to a dopant concentration of ~2%, and both (a-b) are obtained by unfolding the calculated bands due to the 4×4 superlattice artificially introduced in order to simulate the adequate doping concentrations.[53] (c) Schematic diagram showing the bonding and anti-bonding energy levels of Mo d_{z^2} with X p_z orbitals. (d, e) Partial charge densities (shown in yellow) in both the side (left) and top (right) views of N- and P-doped $MoSe_2$, respectively.

Table of Contents

Shallow acceptor of phosphorous doped in $MoSe_2$ monolayer is achieved. P atoms substitute Se in $MoSe_2$, leading to an effective Fermi level shift and confirming the controllable p-type doping. For group-V elements, calculations elucidate the dopant energy level becomes shallower with increasing atomic mass, consistent with experiments.

Keywords: Doping

Yipu Xia, Junqiu Zhang, Zhoubin Yu, Yuanjun Jin, Hao Tian, Yue Feng, Bin Li, Wingkin Ho, Chang Liu, Hu Xu, Chuanhong Jin, and Maohai Xie

Title: Shallow Acceptor of Phosphorous Doped in $MoSe_2$ Monolayer